Journal of
Marine Science and Engineering

MDPI

Article

Floating Behavior of a Composite Bucket Foundation under the Combined Action of Wind and Waves

Xing Zhao [1,2,3,*], Puyang Zhang [3,*], Conghuan Le [3] and Hongyan Ding [3]

[1] Yellow River Institute of Hydraulic Research, YRCC, Zhengzhou 450003, China
[2] Henan Key Laboratory of Ecological Environment Protection and Restoration of Yellow River Basin, Zhengzhou 450003, China
[3] State Key Laboratory of Hydraulic Engineering Simulation and Safety, Tianjin University, Tianjin 300072, China; lch@tju.edu.cn (C.L.); dhy_td@163.com (H.D.)
* Correspondence: 1016205029@tju.edu.cn (X.Z.); zpy@tju.edu.cn (P.Z.)

Abstract: In this study, a composite bucket foundation (CBF) was investigated by taking into account the reflection and refraction effects of waves. A numerical model for the motion responses of the structure under different wave heights and wave periods was built based on the 3D potential flow theory. The model was verified against the test results for analyzing the stability and seakeeping performance of the foundation under the action of waves. Under the combined action of wind and waves, the possible scenarios of floating under wind and waves of different scales and directions were simulated, and the mooring force and motion response peaks and laws of the structure were established, aiming to improve the safety of composite bucket foundation transport and provide technical support for floating construction.

Keywords: composite bucket foundation (CBF); motion response; 3D potential flow theory; MOSES

check for updates

Citation: Zhao, X.; Zhang, P.; Le, C.; Ding, H. Floating Behavior of a Composite Bucket Foundation under the Combined Action of Wind and Waves. *J. Mar. Sci. Eng.* **2022**, *10*, 147. https://doi.org/10.3390/jmse10020147

Academic Editor: José-Santos López-Gutiérrez

Received: 29 December 2021
Accepted: 20 January 2022
Published: 23 January 2022

Publisher's Note: MDPI stays neutral with regard to jurisdictional claims in published maps and institutional affiliations.

Copyright: © 2022 by the authors. Licensee MDPI, Basel, Switzerland. This article is an open access article distributed under the terms and conditions of the Creative Commons Attribution (CC BY) license (https://creativecommons.org/licenses/by/4.0/).

1. Introduction

In recent years, global wind power technology has been greatly developed, and the wind power market has gradually moved towards the development of wind energy at low wind speeds and offshore wind farms. Wind turbine blades are also growing [1–3], and requirements for the construction, transportation, and carrying capacity of foundations are also increasing. The foundation of offshore wind power is mainly divided into two types: fixed and floating. The offshore wind farms currently in operation all use a fixed foundation. Fixed foundations mainly include gravity foundations, single pile foundations, bucket foundations, tripod foundations, and jacket foundations. Floating foundations include spar, tension leg platforms, and semi-submersible foundations. Single-pile foundations, gravity foundations, etc., mostly adopt a step-by-step transportation construction scheme, that is, first use a transport ship to construct the bottom foundation in place, and then use auxiliary facilities such as floating cranes to install the upper fan and tower. The floating foundation can adopt a one-step transportation scheme, that is, after the fan, tower, and floating foundation are installed in the shore dock, the whole is transported to the designated location for anchoring by the tugboat. Due to the structure of the bottom opening of the bucket foundation, it has air-cushion floatation characteristics, so it can also be used for long distance transportation by air floating towing.

The large-diameter wide-shallow composite bucket foundation [4], an improvement of the conventional bucket foundation, is an innovative application in the field of offshore wind power. A honeycomb-type subdivision structure is designed inside the conventional bucket foundation. The composite features of the foundation are mainly embodied in the following aspects: (1) In terms of structural form, the composite bucket foundation comprises a bucket foundation, a composite beam-slab head cover, and an upper load-transfer transition section [5,6]. (2) The structural materials uses prestressed reinforced

concrete (transition section), reinforced concrete with profiled steel sheets (head cover), and steel (bucket wall and subdivision deck). (3) A honeycomb-type subdivision structure is built and installed inside with a negative-pressure piping system. It not only offers bearing strength reserve [7,8], but also satisfies the floating-dropping-leveling requirements [9–14]. As a design and construction technique independently developed by China, the new and improved foundation is capable of realizing onshore prefabrication, self-floating towing, and negative-pressure dropping, and is characterized by convenient noiseless construction, lowered cost, reduced offshore operation time, batch prefabrication, high recyclability, etc. [15–17]. In October, 2010, the first 2.5 MW composite bucket foundation prototype was completed and put into service in Qidong, Jiangsu Province, and the floating of the foundation, the dropping after installation, and the unit assembling of the wind turbine generator were finished, as shown in Figure 1. In 2017, the one-step offshore transport and installation of the foundation, tower, and head of the first 3 MW composite bucket foundation were completed in the Xiangshui Wind Farm of China Three Gorges New Energy Corp. In 2019, the one-step transport and installation of two 6.45 MW units were completed in the Dafeng Wind Farm of China Three Gorges New Energy Corp [18–20].

(**a**) (**b**)

(**c**)

Figure 1. Floating behavior of the composite bucket foundation: (**a**) Lifting; (**b**) Hoisted into the water; (**c**) Floating.

In the application and promotion of the composite bucket foundation, its air-floating characteristic and induced dropping constitute two aspects essential for realizing its structural advantages [21–23]. Zhang [24] established the air floating towing model of bucket foundation structure by using MOSES, focused on the changes of floating state and high initial stability of the structure, and carried out frequency domain and time domain analysis. Zhang [25] analyzed the influence of subdivision plate on structural towing resistance through a hydrostatic towing test. The numerical results are further verified, and the motion characteristics of bucket foundation towing are analyzed. Ding [26] designed a one-step transport and installation ship to transport and install the bucket foundation and the upper fan as a whole, and studied the effects of ship speed, wave height, and wind speed on the floating performance of the structure. The structural stability of the air-floating towing of the composite bucket foundation in the floating state and its dynamic responses under the action of waves are also worth exploring for in-depth investigation. This paper focuses on the CBF, an environmentally friendly foundation structure suitable for the development of offshore wind farms in China, and conducts research on the safety mechanism of air floatation. First, the scale foundation test and the numerical calculation of MOSES are used. The towing force, pitch angle, and air pressure during towing are compared and analyzed to verify the effectiveness of model experiments and numerical calculation methods. Afterwards, the numerical calculation method was used to study the floating behavior of the CBF under the combined action of wind and waves. By analyzing the floating simulations that may actually encounter winds and waves of different levels and directions, the towing force, peak value, and law of motion response of the structure were summarized. It aims to improve the safety of the CBF transportation and provide technical support for a structure's floating construction.

2. Test Model

The test model was made of organic glass and designed by a model/prototype ratio of 1:35 under the principle of geometric similarity. The model parameters are listed in Table 1. The counterweight was designed according to the principle of gravity similarity, and the weight of iron block was 32.8 kg. Referring to the principle of inertia force similarity, Figure 2 shows four balancing weights used, each with a mass of 8.2 kg, a height of 27.5 cm, and 22 cm away from the center of the head cover. Two small openings are set at the top of each room, and a connected air pump is used for controlling the air water ratio and structural leveling. The other connected air pressure sensor is used to measure the air pressure in the room. Figure 3 illustrates the subdivision of the composite bucket foundation. The structure was lifted to the designated position in the harbor basin using a crane. According to the actual towing of the prototype, a Y-type towing cable is used for towing. Two towing points on the bucket wall are set at the position 20 cm away from the bottom of the bucket. The Y-shaped angle is 90° and the two towing points are located in the center of room 1 and room 2, respectively.

Table 1. Model parameters.

	Diameter/m	Length of Subdivision Deck/m	Height/m	Weight	Height of Center of Gravity/m	Radius of Gyration/m
Prototype	35	8.75	10	3000 t	3.9	10.6
Test model	1	0.25	0.285	70 kg	0.11	0.3

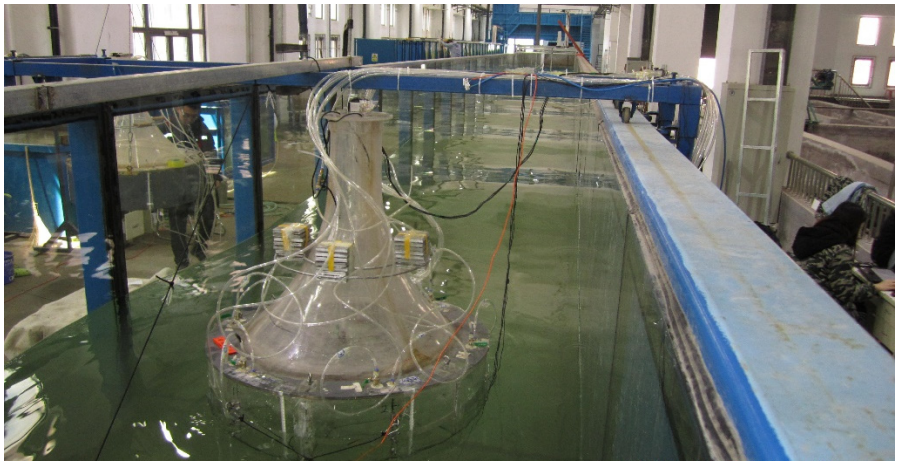

Figure 2. Experimental model.

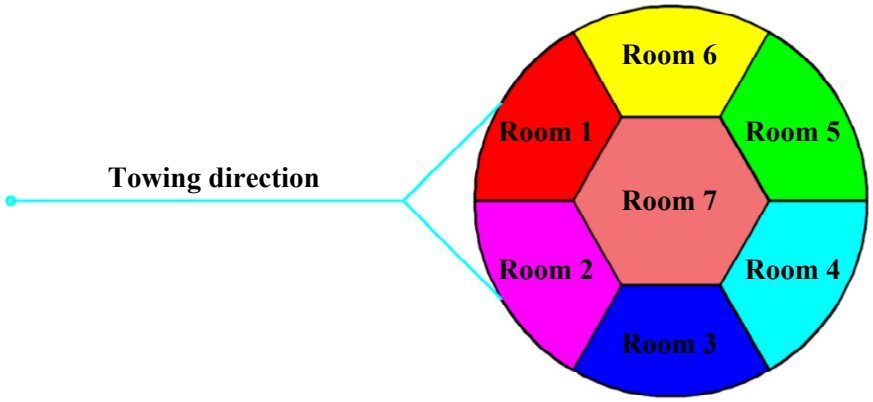

Figure 3. Schematic diagram of the subdivision of the composite bucket foundation.

The test arrangement is shown in Figure 4. The towing test was carried out in the port laboratory of Tianjin University. The pool is 90 m long, 2 m wide and 1 m deep. Low inertia AC servo wave plate wave maker is used to make waves. The wave period can be controlled within 0.5~5 s, and the maximum wave height is 0.5 m. A wave energy absorption device is installed at the end of the pool. A tension sensor is installed on the cable to measure the towing force during the towing process; seven gas pressure sensors are respectively arranged on the top of the rooms of the CBF to measure the internal gas pressure; a gyro is set on the flange position at the top of the transition section to measure the 6 degrees of freedom movement of the structure. After being in place, inflate the room to make the foundation float on the water surface. By controlling the air water ratio in the room, the draft of the bucket foundation is adjusted to the specified position. After that, the wave towing test is carried out. The incident wave conditions refer to the measured wave data (see Table 2) of a certain sea area in Jiangsu Province. The towing speed refers to the towing speed selected in the actual project. At the same time, the influence of different irregular waves on the structural motion response is considered.

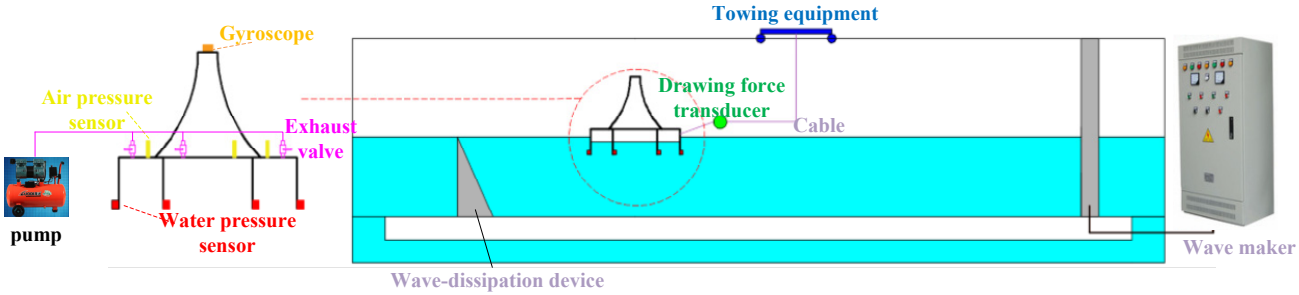

Figure 4. Test arrangement.

Table 2. Wave parameter.

Direction	Wave Height (m)	Wave Period (s)	Wave Length (m)
N-NNE	1.87	8.09	48.48
NE-ENE	1.89	9.75	59.35
E-ESE	1.92	9.87	60.07
SE-SSE	1.68	9.05	54.45

3. Numerical Simulation Settings

3.1. Theory

The towing system of the CBF includes the front tug, the central cable, and the rear CBF, which is a complex system of "gas-liquid-solid" coupling. In the full coupling analysis, this article uses the hydrodynamic analysis software MOSES for programming, modeling, and calculation. The software uses a scripting language to establish the tug and the CBF, and meshes the structure. MOSES is a software tool that integrates marine engineering modeling, simulation, and analysis. The software has three built-in hydrodynamic theories for calculating hydrodynamic loads: Morrison's equation, strip theory, and three-dimensional diffraction theory. In this paper, the three-dimensional diffraction theory is used.

Assuming that the fluid is an ideal fluid that is inviscid and incompressible, the wave motion is a potential motion with a velocity potential $\Phi(x, y, z, t)$, and its relationship with the velocity vector U is expressed as Equation (1):

$$U(x, y, z, t) = \nabla\Phi(x, y, z, t) \tag{1}$$

Obviously, the velocity potential should satisfy the Laplace equation, that is, Equation (2):

$$\nabla^2\Phi(x, y, z, t) = 0 \tag{2}$$

At these positions (the calculation domain, seabed level, free liquid surface, structural surface, and infinity), it should satisfy the following Equation (3):

$$\begin{cases} \nabla^2\Phi(x, y, z, t) = 0 \\ \frac{\partial\Phi}{\partial z} = 0, z = -d \\ \frac{\partial^2\Phi}{\partial t^2} + g\frac{\partial\Phi}{\partial z} = 0, z = 0 \\ \frac{\partial\Phi}{\partial N} = 0 \\ \nabla\Phi(x, y, z, t) \to 0, r \to \infty \end{cases} \tag{3}$$

where d is the water depth, N is the unit normal vector of structural plane.

3.2. Wave Spectrum

The random wave spectrum used in the numerical calculation is the JONSWAP spectrum, which is suitable for the spectrum with limited wind range, as shown in Equation (4):

$$S(\omega) = \alpha g^2 \omega^{-5} \exp\left[-\frac{5}{4}\left(\frac{\omega_m}{\omega}\right)^4\right] \gamma^{\exp\left[-\frac{(\omega-\omega_m)^2}{2\sigma^2\omega_m{}^2}\right]} \quad (4)$$

where α is the energy scale parameter, $\alpha = 0.076\langle gx/U^2\rangle^{-0.22}$; x is the wind range; U is the average wind speed; ω_m is the spectral peak frequency, $\omega_m = 22(\ g/U)(gx/U^2)^{-0.33}$; γ is the peak lift factor, which is 3.3; σ is the peak shape parameter, when $\omega \leq \omega_m$, $\sigma = 0.07$, when $\omega > \omega_m$, $\sigma = 0.09$.

3.3. Current Load and Wind Load

The current load on the composite bucket foundation is shown in Equation (5) below:

$$F_{\text{current}} = \frac{1}{2}\rho C_d A u^2 \quad (5)$$

where F_{current} is the current load, ρ is the seawater density, C_d is the towing coefficient, A is the projected area in the direction of flow velocity, and u is the relative velocity of the flow compared to the towing motion of the CBF.

When the sea breeze blows through the CBF, the wind load it receives is shown in Equations (6) and (7) below:

$$F_{\text{wind}} = \frac{1}{2}C_W \rho_a A_a V^2 \quad (6)$$

$$M_{\text{wind}} = \frac{1}{2}C_W \rho_a A_a V^2 H \quad (7)$$

where F_{wind} is wind force, M_{wind} is wind moment, C_W is wind load factor, ρ_a is air density, and A_a is the projected area of the CBF in the direction of wind speed (in this paper, it refers to the projected area of the transition section of the CBF). V is the relative speed of the wind compared to the towing motion of the CBF. H is the distance from the wind action point to the center of gravity of the CBF.

3.4. Numerical Simulation Conditions

In the towing test of the composite bucket foundation, model scale, test site, and other conditions inevitably affect the test results, making it impossible to faithfully reflect its motion characteristics in a sea area. To verify the accuracy of the model test, this study used MOSES software to build the composite bucket foundation prototype. Subdivision and room numbering were consistent with the test. Each room was drilled at the bottom with air holes to simulate the openings at the bottom of the foundation, and different water-air ratios and air pressure were adopted for different rooms to adjust the draft. In the calculation process, the air pressure value can be converted through the water pressure difference inside and outside the bucket. The flexible connector "h_cat" is used to simulate the cable and the cable diameter is 80 mm. The safe length of the main towing line is 120 m. The pull on the main towing line is the dragging forces, including the action of wind, wave, and current load. Converted by the same scale, the test water depth was equivalent to a real water depth of 35 m. Side walls were erected on the test site for the simulation of basin boundary. The wave type is regular wave, and the grid width is 1 m. Figure 5 shows the MOSES model. The test results were converted to prototype values based on the similarity relationships for a comparison with the numerically simulated values. Table 3 summarizes the regular wave test conditions corresponding to the working conditions of the prototype.

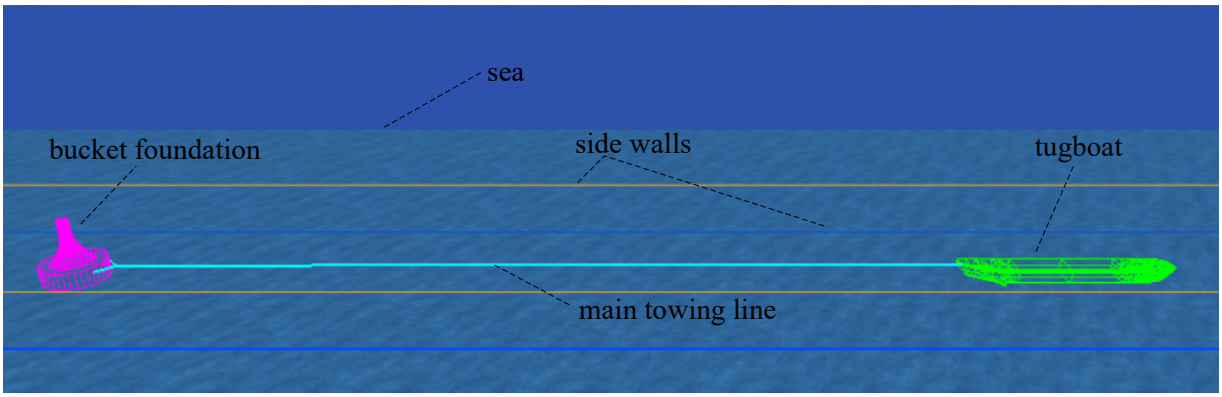

Figure 5. Schematic diagram of the towing simulation using MOSES.

Table 3. Towing conditions of the composite bucket foundation prototype.

Towing Condition	WavePeriod/s	Wave Height/m	Wave Direction	Towing Speed/m/s	Draft/m	Ratio of Air and Water in the Room	Mooring Position
S1	9	1	Head sea	1.5	7	1.57:1	High
S2	9	2	Head sea	1.5	7	1.57:1	High
S3	9	3	Head sea	1.5	7	1.57:1	High
S4	6	2	Head sea	1.5	7	1.57:1	High
S5	12	2	Head sea	1.5	7	1.57:1	High

3.5. Static Stability Verification

In order to verify the accuracy of the numerical model, adjust the draft of the test model and the numerical model to 7 m. After the structure is stable, give it an initial roll angle and heave displacement, and the structure will roll and heave. Set an investigation point at the top center of the bucket foundation to obtain the decay process of the roll angle and heave displacement of this point. The normalized results are shown in Figure 6. It can be seen from the figure that the roll and heave decay obtained by numerical calculation is basically consistent with the results of model test. The roll and heave natural periods of the structure are 11.8 s and 7.9 s, respectively.

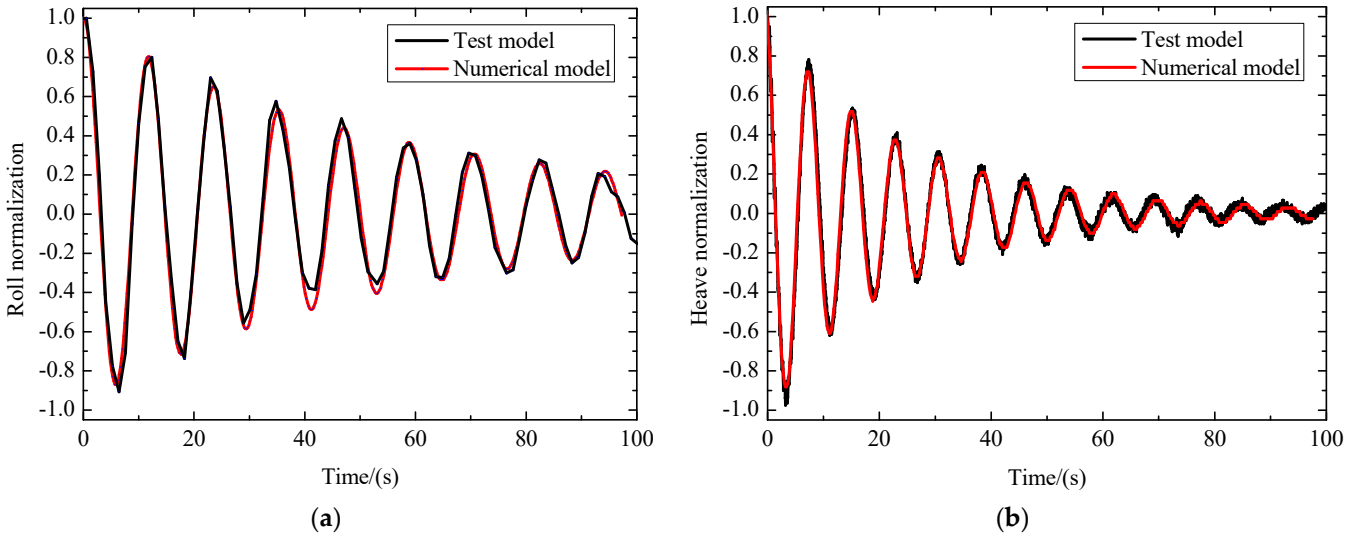

Figure 6. Roll and heave decay curve: (**a**) Roll; (**b**) Heave.

4. Analysis

4.1. Cable Dragging Forces

A duration of 3000 s was used for the time-domain calculation of towing. For the clarity of data, the calculation results within the range 2700–3000 s were selected after the stabilization of towing motion. Figures 7 and 8 show the variations in the cable dragging force of the composite bucket foundation under different wave parameters. Figure 9 shows a comparison of the tested and numerically simulated cable dragging forces.

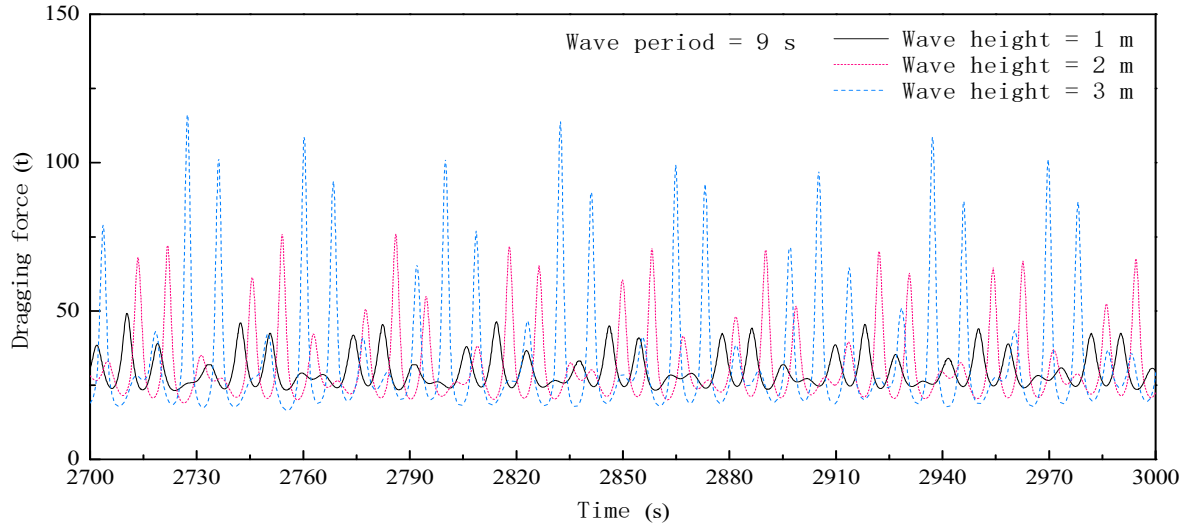

Figure 7. Effect of the wave height on the numerically simulated cable dragging force.

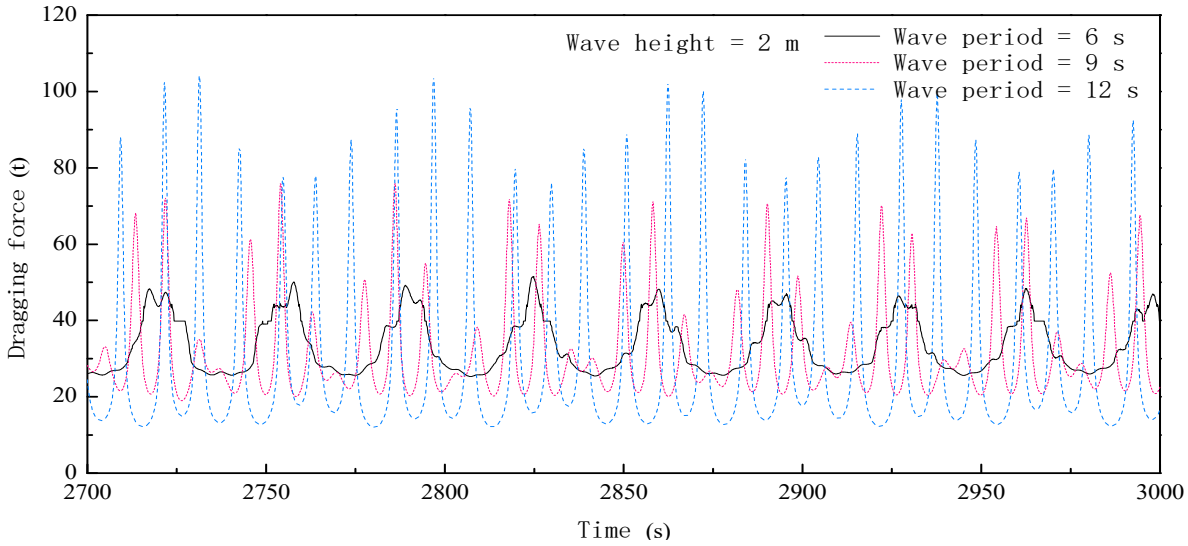

Figure 8. Effect of wave period on the numerically simulated cable dragging force.

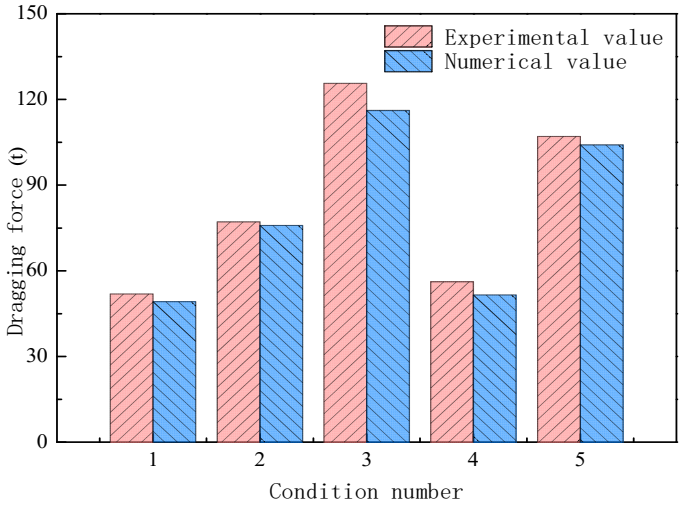

Figure 9. Comparison of the tested and numerically simulated cable dragging forces.

With increasing wave height, the peak cable dragging force of the structure increased. At a wave height of 1 m, its maximum dragging force was 48 t, which reached 79 t at a wave height of 3 m. With the extension of wave period, the peak cable dragging force of the structure also presented an increasing trend. At a wave period of 6 s, its maximum dragging force was 34 t, which reached 103 t at 12 s. The trend and range of the cable dragging force of the foundation varying with wave parameters in the towing motion basically matched with those of the test, thus verifying the reliability of the numerically simulated cable dragging forces.

4.2. Pitch Angles

The motion of the structure in floating state was dominated by pitch. Figures 10 and 11 show the variations in the pitch angle of the composite bucket foundation under different wave parameters. Figure 12 shows a comparison of the tested and numerically simulated pitch angles.

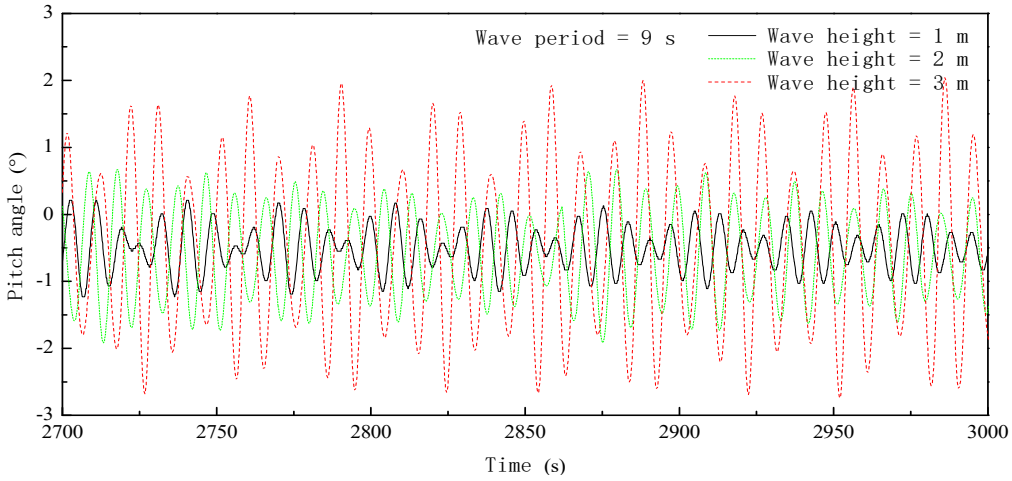

Figure 10. Effect of wave height on the numerically simulated pitch angle.

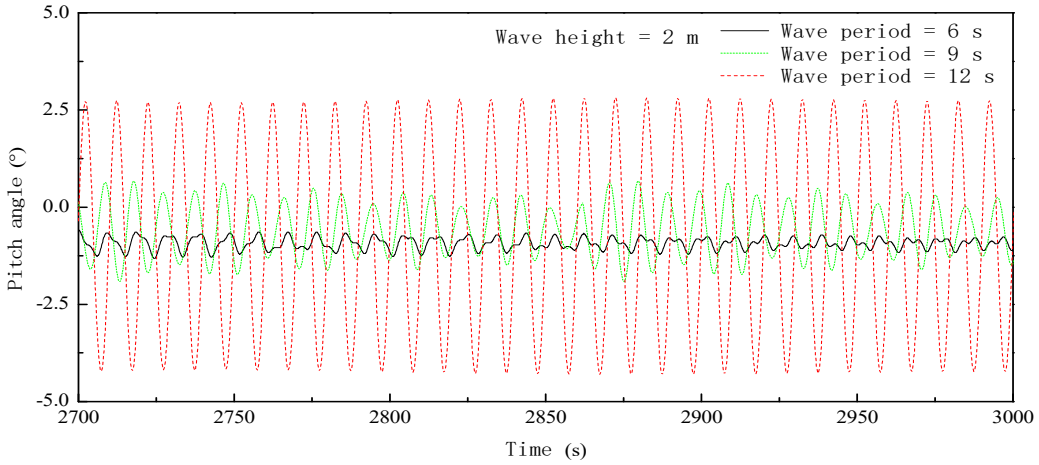

Figure 11. Effect of wave period on the numerically simulated pitch angle.

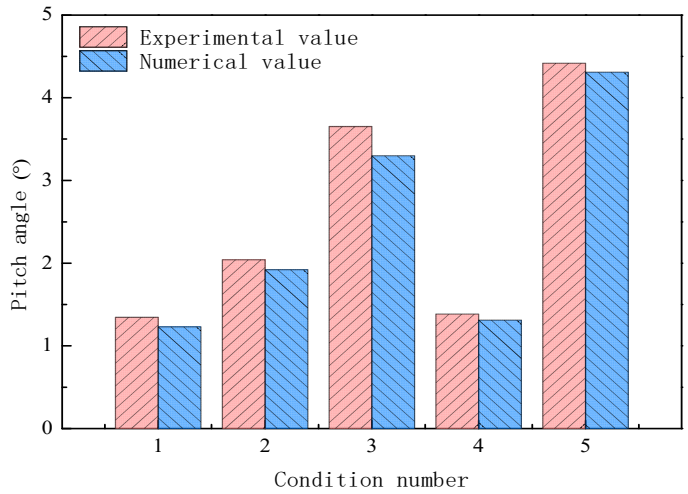

Figure 12. Comparison of tested and numerically simulated pitch angles.

With increasing wave height, the pitch angle of the structure increased. At a wave height of 1 m, the maximum forward pitch angle of the structure was 0.65°, which reached 2.7° at 3 m wave height. With increasing wave period, the pitch angle of the structure also presented an increasing trend. At a wave period of 6 s, the maximum forward pitch angle of the structure was 0.7°, which reached 4.1° at 12 s. The trend and range of the pitch angle of the foundation varying with wave parameters in the towing motion basically matched with those of the test, verifying the reliability of the numerically simulated pitch angles.

4.3. Air Pressures

Figures 13 and 14 show the variations in the air pressure of the composite bucket foundation under different wave parameters. Figure 15 shows a comparison of the tested and numerically simulated air pressures.

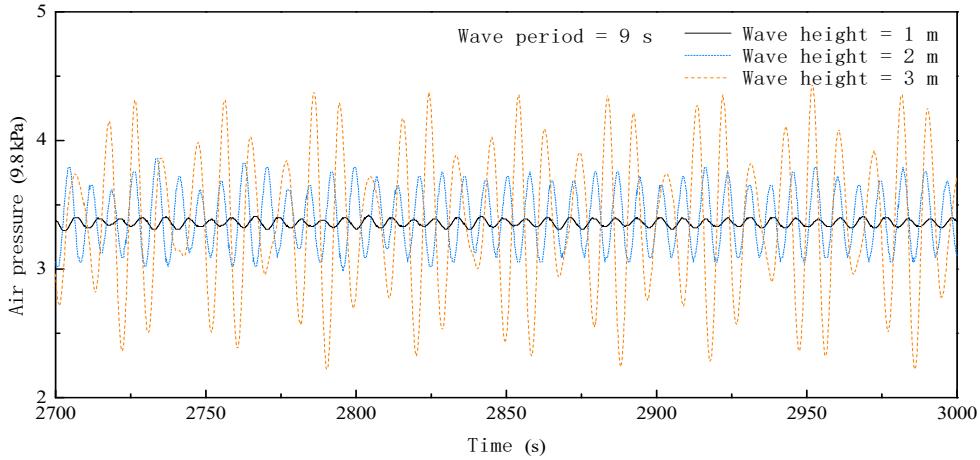

Figure 13. Effect of the wave height on the numerically simulated air pressure of room 1.

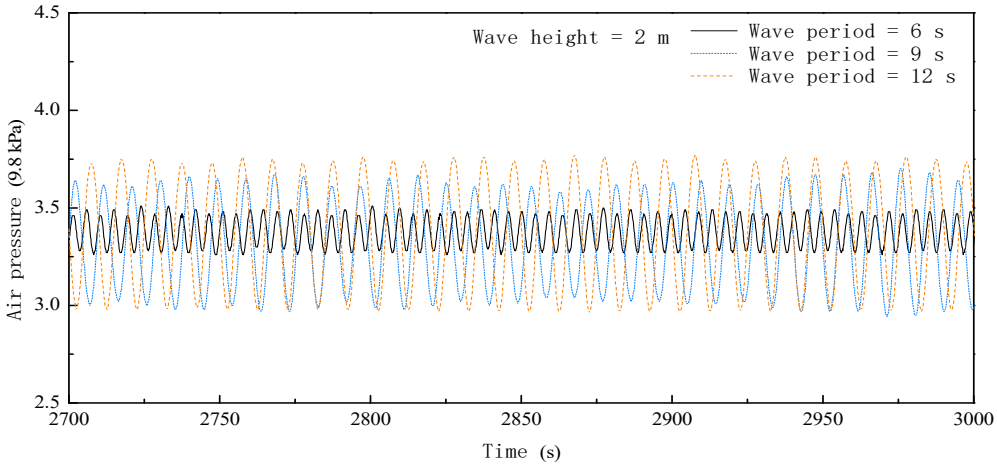

Figure 14. Effect of the wave period on the numerically simulated air pressure of room 1.

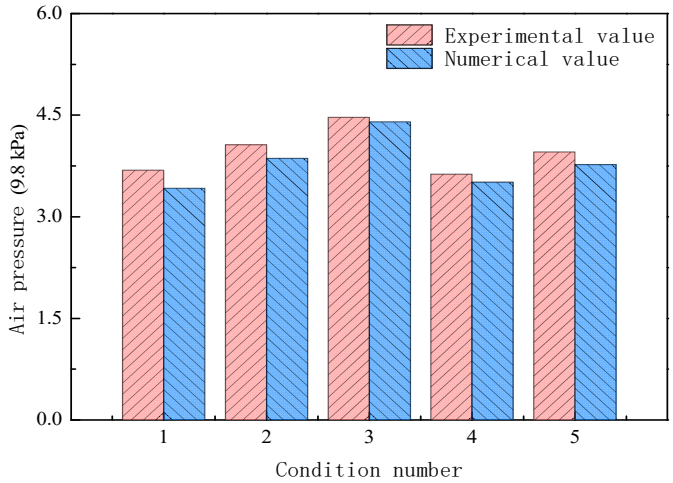

Figure 15. Comparison of the tested and numerically simulated air pressures.

With increasing wave height, the air pressure of room 1 fluctuated within a wider range. At a wave height of 1 m, the air pressure (converted to water head height) of room 1 fluctuated within the range 3.3–3.4 m and at 3 m, it fluctuated within the range 2.2–4.3 m. With increasing wave period, the air pressure of room 1 also presented an increasing trend. At a wave period of 6 s, the air pressure of room 1 fluctuated within the range 3.3–3.5 m; at

12 s, it fluctuated within the range 2.9–3.8 m. The trend and range of the air pressure of the foundation varying with wave parameters in the towing motion basically matched with those of the test, verifying the reliability of the numerically simulated air pressure.

From the above test and calculation results of towing force, pitch angle, and air pressure, it can be seen that the variation rules of the three parameters with wave parameters are consistent. The change of cable force and air pressure is caused by the movement of the structure. When the fluctuation range of pitch angle becomes larger, the impact force will be produced on the trailer, which will lead to the fluctuation of wave force. The internal air pressure (P_a) in the room can be calculated from Equation (8) below.

$$P_a = P_0 + \rho_w g h_w \tag{8}$$

where P_0 is the standard atmospheric pressure, ρ_w is the density of seawater, h_w is the water level difference between inside and outside the bucket.

With the increase of the maximum pitch angle, the maximum water level difference between inside and outside the No. 1 room will also increase, so the air pressure in the room will also increase. When the wave height increases, the wave force of the structure will also increase, so the swing of the structure will be greater. The influence of wave period is mainly related to the pitch natural period of the structure itself. When the wave period is close to the natural pitch period of the structure, the swing angle of the structure is the largest. Previous research results show that the natural pitch period of the bucket foundation prototype is 10~12 s. Therefore, when the wave period increases (from 6 s to 12 s), the pitch angle of the structure increases, and the towing force and air pressure also increase.

4.4. Floating Behavior under the Combined Action of Wind and Waves

The environmental load factors affecting the composite bucket foundation in the towing motion mainly included wind and waves. In this study, wind simulation was performed using average wind, and wave simulation was conducted using the random waves generated by the JONSWAP wave spectrum.

To identify the effects of environmental factors on the floating behavior of the composite bucket foundation, five groups of sea conditions were selected for 3000 s towing simulation, which basically covered all the possible sea conditions in practical towing operation in the sea areas of Fujian Province and Jiangsu Province, as listed in Table 4. The towing speed was set as the field towing speed of 3 sea miles per hour, the draft was set at 7 m, and the height of the mooring point was set at 7 m above the water plane. According to different wind levels and wave directions, it is divided into the following five working conditions (TH1-TH5). Under 3,5,7 level wind, TH1-TH3 were selected to compare the effects of different wind and wave environments on floating. TH3-TH5 were used to compare the effects of head sea, beam sea, and following sea conditions on floating. For the sake of clear presentation, the time–history curves of the irregular wave height selected the interval of 600 s, as illustrated in Figure 16.

Table 4. Sea conditions for towing simulation.

Environmental Parameter	TH1	TH2	TH3	TH4	TH5
Wind level	3	5	7	7	7
Average wind speed/m/s	5	10	17	17	17
Significant wave height/m	1	2	2.5	2.5	2.5
Peak spectral period/s	9.8	10	10.5	10.5	10.5
Towing speed/m/s	1.5	1.5	1.5	1.5	1.5
Wave direction	180	180	180	90	0

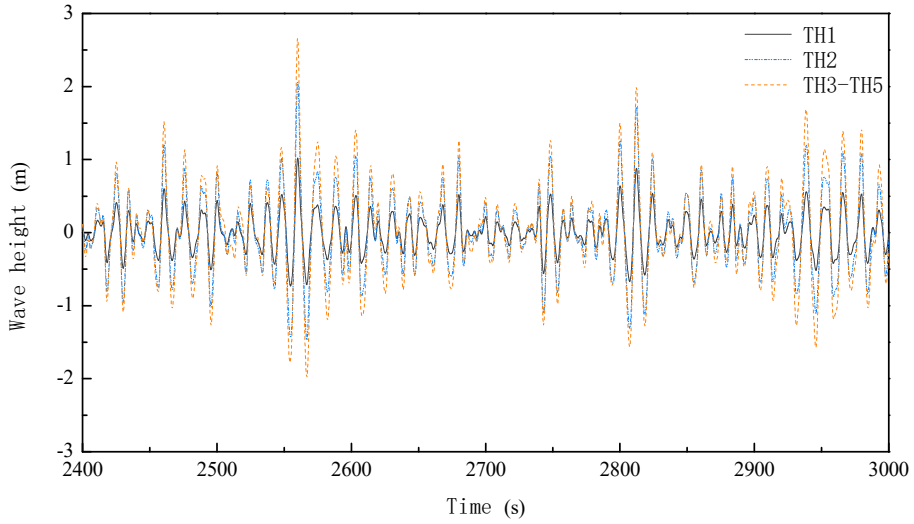

Figure 16. Time–history curves of wave height under different sea conditions.

Figure 17 shows the time–history curves of cable dragging force under 3,5,7 level wind. Figure 18 presents the time–history curves of cable dragging force under different wave directions. Figure 19 shows a visual presentation of the statistics of cable dragging force under different sea conditions. Clearly, the maximum cable dragging forces of the foundation under 3,5,7 level wind were 138 t, 212 t, and 257 t, respectively. The average cable dragging forces in the three environments were basically consistent; however, the standard deviations of numerical fluctuations presented an ascending trend. Under different wave directions, the maximum cable dragging force occurred under head sea condition, followed by that under beam sea condition (245 t), while the minimum one was observed under following sea condition (221 t). Thus, an accurate numerical simulation of cable dragging force is conducive to the reasonable selection of towing motors and the lowering of construction cost in practical towing.

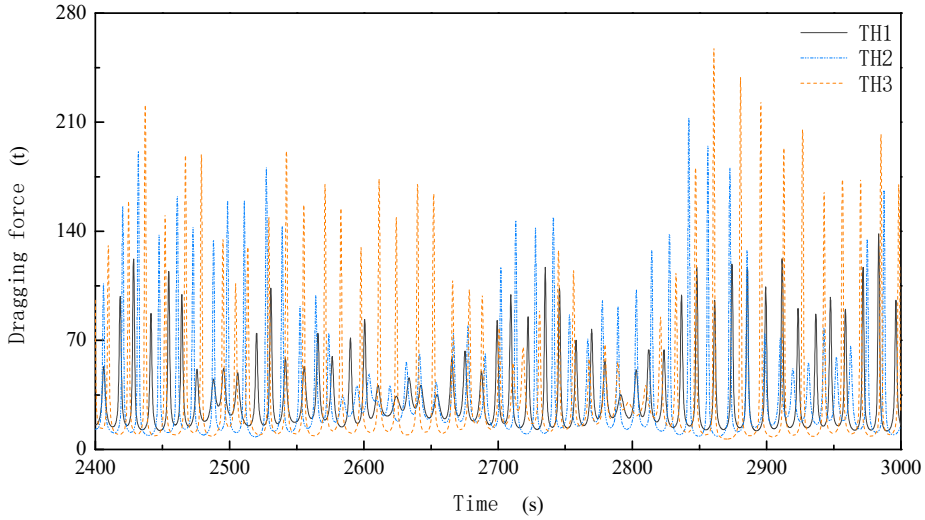

Figure 17. Time-history curves of cable dragging force under different wave heights.

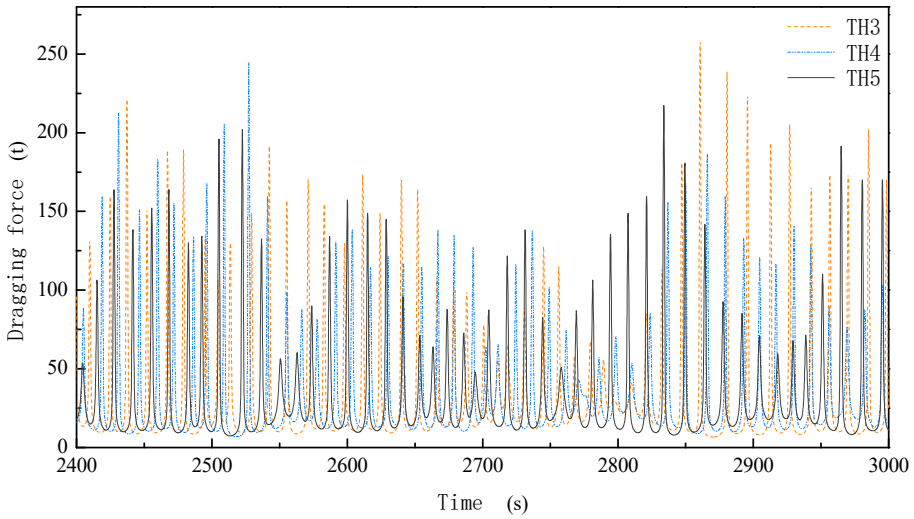

Figure 18. Time-history curves of cable dragging force under different wave directions.

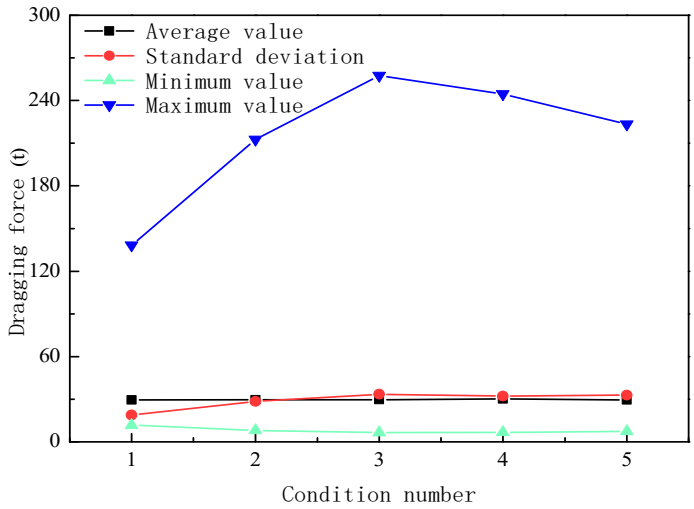

Figure 19. Statistics of cable dragging force under different sea conditions.

Figures 20 and 21 show the time–history curves of the pitch angle and heave of the foundation in the towing motion under different sea conditions, respectively. For the sake of clarity, the time–history curves were generated at an interval of 300 s, while the statistics adopted a full time domain of 3000 s, as illustrated in Figures 22 and 23. A negative value denotes a forward pitch angle, while a positive value represents a backward pitch angle. As shown in Figures 22 and 23, the ranges of forward and backward pitch angles under 3,5,7 level wind increased gradually, with the maximum forward pitch angles were 2.3°, 3.1°, and 3.2°, respectively. Under force 7 wind and waves, the maximum pitch angle was observed under the beam sea condition (3.5°), while the pitch angles under following sea and head sea conditions were close to each other (about 3.3°). The average pitch angle in the towing motion under different sea conditions was −0.5°, indicating it as forward towing.

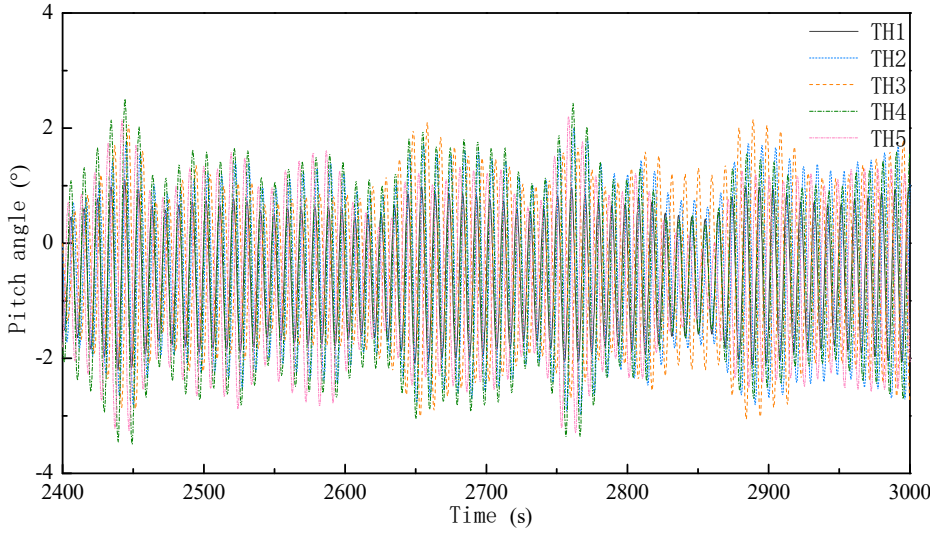

Figure 20. Time–history curves of the pitch angle under different sea conditions.

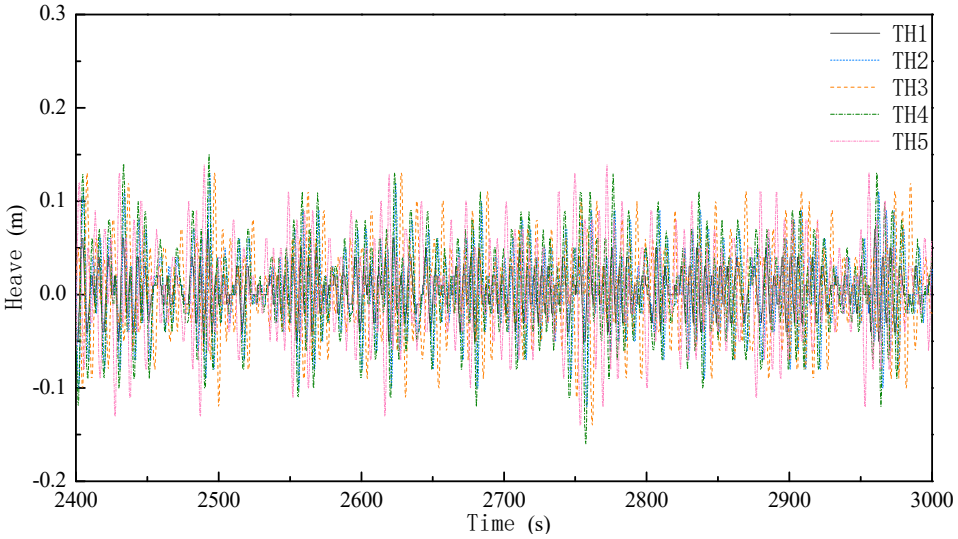

Figure 21. Time–history curves of heave under different sea conditions.

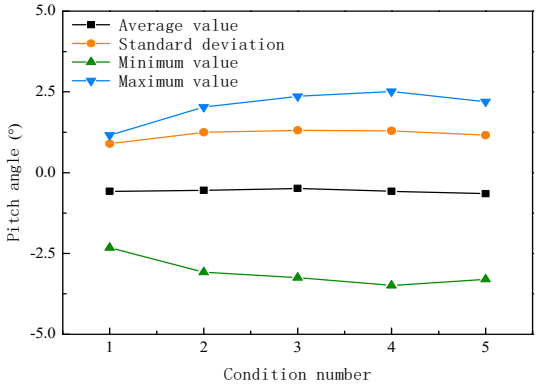

Figure 22. Statistics of the pitch angle under different sea conditions.

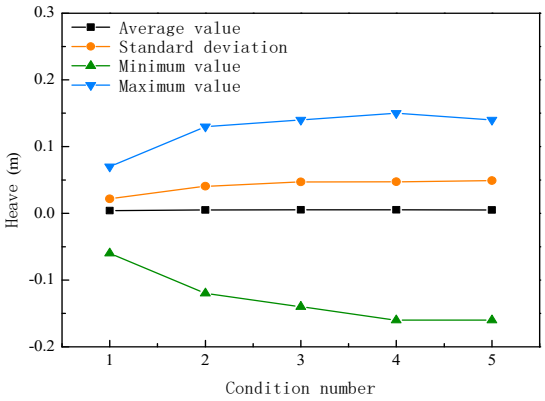

Figure 23. Statistics of the heave under different sea conditions.

The heave value of the foundation was negative when moving downwards and positive when moving upwards. Its heave ranges in upward and downward motion under 3,5,7 level wind increased gradually, with the maximum heave values were 0.07, 0.13, and 0.14 m, respectively. Under force 7 wind and waves, the maximum heave value occurred under beam sea condition (0.15 m), while the heave values under following sea and head sea conditions were close to each other (approximately 0.14 m). The motion responses of the foundation increased with increasing wind and wave scale and were affected to a lesser extent by wave direction; however, towing under beam sea condition should be avoided as far as possible.

Figures 24–27 show the time–history curves of the air pressures of rooms 1, 5, 6, and 7 when the composite bucket foundation was towed under 3,5,7 level wind. Figure 28 shows a visual presentation of the air pressure statistics of various rooms under different sea conditions. Clearly, under 3 level wind, the air pressure of room 1 fluctuated within the range 3–3.7 m; under 5 level wind, it fluctuated within the range 2.79–3.9 m; under 7 level wind, it fluctuated within the range 2.7–3.92 m. Under different wave directions, the fluctuation range of the air pressure of room 1 did not change much. However, the fluctuation ranges of the air pressures of rooms 1, 5, and 6 narrowed gradually, and those of rooms 6 and 7 had smaller standard deviations.

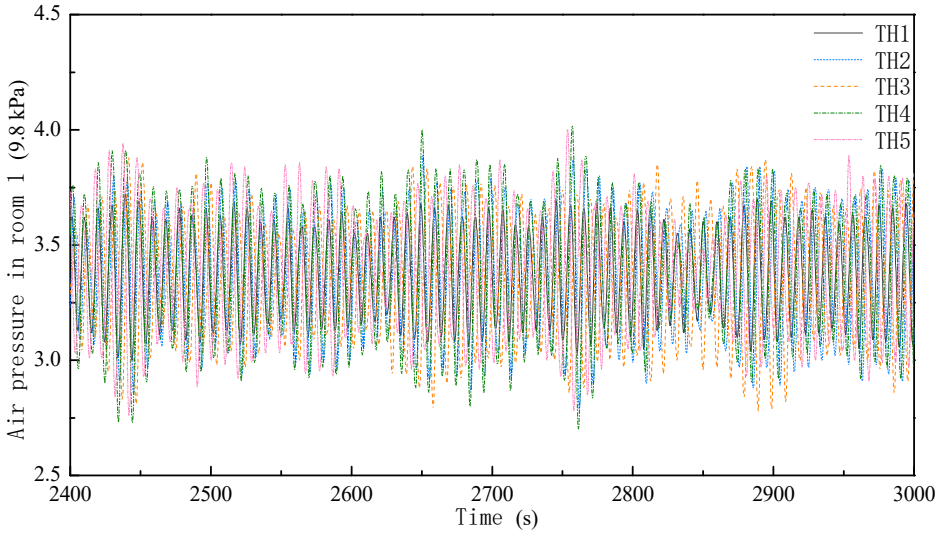

Figure 24. Time–history curves of the air pressure of room 1 under different sea conditions.

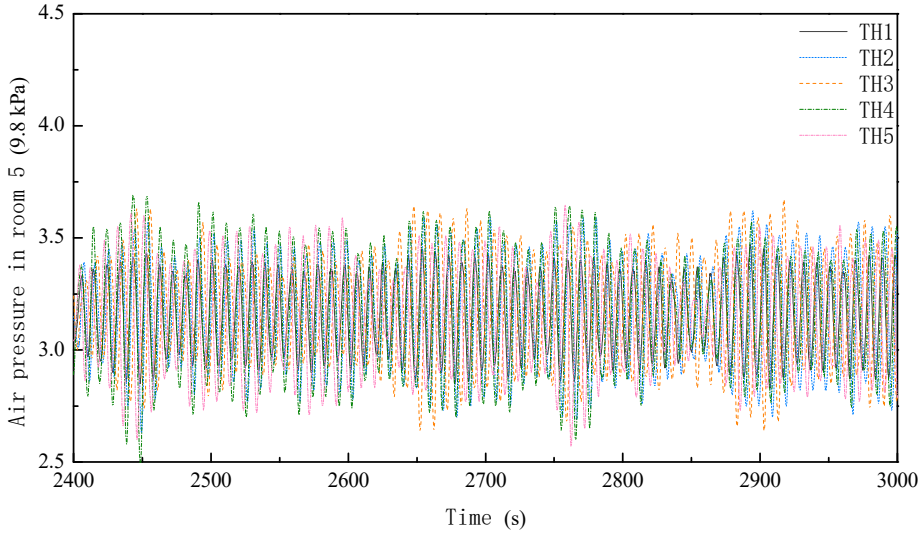

Figure 25. Time–history curves of the air pressure of room 5 under different sea conditions.

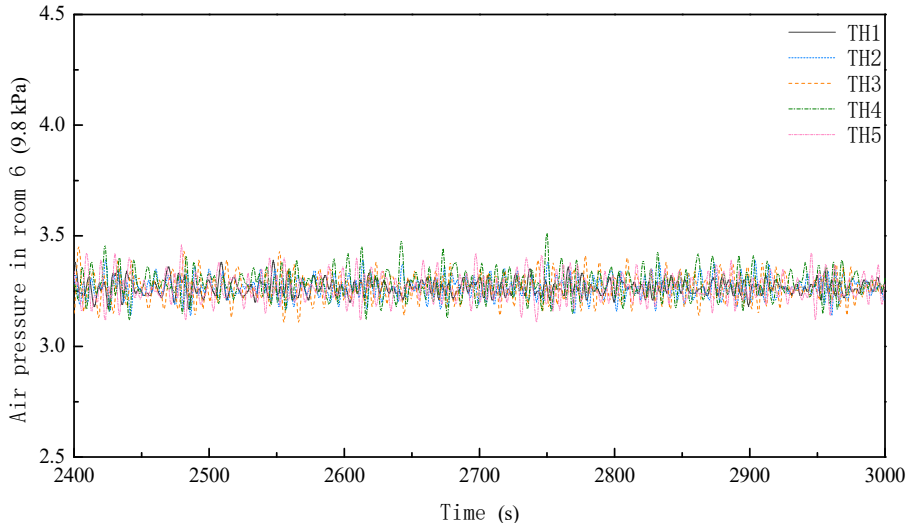

Figure 26. Time–history curves of the air pressure of room 6 under different sea conditions.

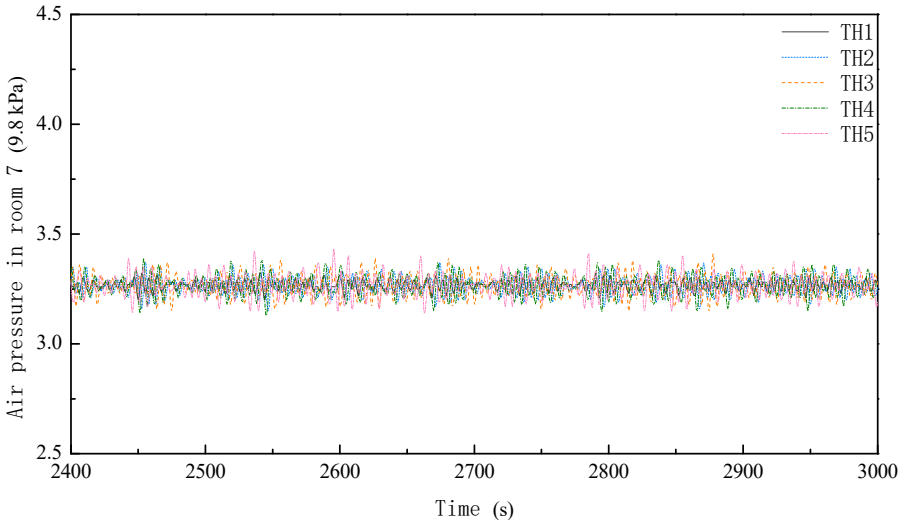

Figure 27. Time–history curves of the air pressure of room 7 under different sea conditions.

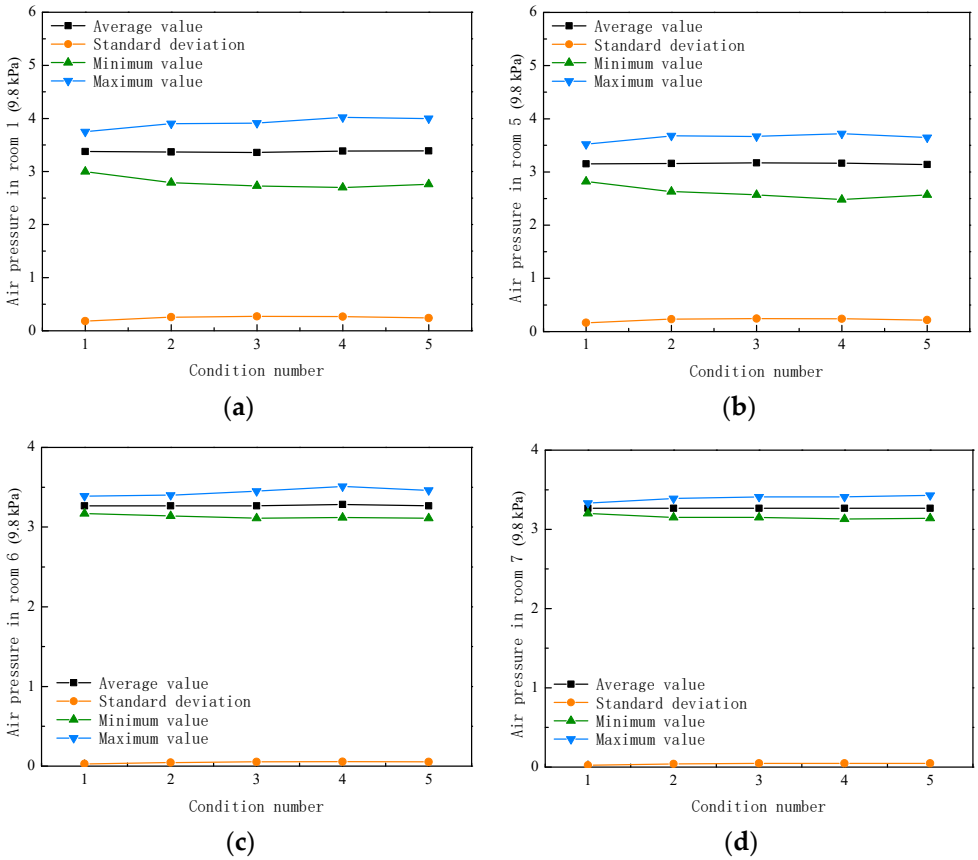

Figure 28. Air pressure statistics of various rooms under different sea conditions: (**a**) Air pressure of room 1; (**b**) Air pressure of room 5; (**c**) Air pressure of room 6; (**d**) Air pressure of room 7.

It can be seen from the above calculation results that the wave height, period, and wind speed of the first three working conditions are slightly increased, so the calculation results are similar to the previous test results. With the increase of wave height, period and wind speed, the maximum values of pitch angle, air pressure and towing force of the structure will increase. In the last three conditions, the wind speed, wave height, period and speed remain unchanged, only the wave direction is different. Due to the different wave directions, the wave encounter period of the structure is slightly different, but the difference is not big, so the pitch angle and air pressure change little. The calculation of towing force includes current resistance, wind resistance and wave slapping force. The wave slapping force will change with the change of wave direction, so the towing resistance of the structure will change. The total resistance is the largest in the head sea towing, the minimum in the following sea towing, and the middle in the beam sea towing.

5. Conclusions

The numerical simulation of a composite bucket foundation was preformed based on 3D potential flow, linear wave, diffraction, and radiation theories. The main conclusions of this study are as follows:

(1) The towing test model and MOSES numerical model of bucket foundation are established. Through the free decay test, it is obtained that the roll and heave decay obtained by numerical calculation are basically consistent with the results of model test. When the draft is 7 m, the natural periods of roll and heave of bucket foundation are 11.8 s and 7.9 s, respectively.

(2) In regular wave towing, the values and fluctuation range of dragging force, pitch angle and air pressure of bucket foundation increase with the increase of wave height or wave period. Combined with the experimental and numerical results, it can be

seen that the increase of wave height will increase the wave force of the structure, and then cause greater swing and air pressure change of the structure. With the increase of wave period, it will gradually approach the swing natural period of the structure, resulting in the increase of the swing of the structure, which will lead to the increase of the fluctuation range of dragging force and air pressure. The numerical simulation is in good agreement with the values in the test, which further verifies the reliability of the numerical simulation.

(3) Taking into account the combined action of wind and waves, towing simulation was performed under 3,5,7 level wind. The average value of the drag force in the three environments is basically the same, but the standard deviation of the fluctuation of the value shows an increasing trend, and the maximum values of the towing force are 138t, 212t, and 257t, respectively. The direction of the wave has a greater influence on the towing force. Under different wave directions, the maximum cable dragging force occurred under the head sea condition, followed by that under beam sea condition (245 t), while the minimum forces (221 t) was observed under the following sea condition. The calculation of the towing force helps to reasonably select the towing horsepower in the actual towing, reduce the construction cost, and improve the towing efficiency.

(4) When the draught is 7 m and the tether point is at sea level, the CBF will show a forward tilt during towing under 3,5,7 level wind, and the maximum forward tilt angles are 2.3°, 3.1°, and 3.2°, respectively. The maximum pitch angle was observed under the beam sea condition (3.5°), while the pitch angles under the following sea and head sea conditions were close to each other (approximately 3.3°).

(5) As the level of wind and waves increases, the maximum heave value of the foundation also increases—0.07 m, 0.13 m, and 0.14 m, respectively,. The maximum heave value was observed under the beam sea condition (0.15 m), while the heave values under the following sea and head sea conditions were close to each other (approximately 0.14 m). It can be seen that the motion response of the CBF increases with the increase of the wind and wave level, and the direction of the wind and wave has little effect on it. However, towing should be avoided under the beam wind and beam sea condition as much as possible.

(6) As the level of wind and waves increases, the fluctuation range of the air pressure also increases significantly, and the fluctuation range of the atmospheric pressure of room 1 does not change much under different wave directions.

Author Contributions: Conceptualization, P.Z., H.D. and C.L.; Methodology, P.Z. and X.Z.; Software, X.Z. and C.L.; validation, P.Z., X.Z. and H.D.; Formal Analysis, X.Z. and P.Z.; Writing—Original Draft Preparation, X.Z. and P.Z.; Writing—Review & Editing, P.Z. and X.Z.; Supervision, H.D., C.L. and P.Z.; Project administration, H.D. and P.Z.; Funding acquisition, H.D. and P.Z. All authors have read and agreed to the published version of the manuscript.

Funding: This research was supported by the National Natural Science Foundation of China (No. 52171274).

Institutional Review Board Statement: Not applicable.

Informed Consent Statement: Not applicable.

Data Availability Statement: Not applicable.

Conflicts of Interest: The authors declare no conflict of interest.

References

1. Tarfaoui, M.; Shah, O.R.; Nachtane, M. Design and optimization of composite offshore wind turbine blades. *J. Energy Resour. Technol.* **2019**, *141*, 051204. [CrossRef]
2. Tarfaoui, M.; Nachtane, M.; Boudounit, H. Finite element analysis of composite offshore wind turbine blades under operating conditions. *J. Therm. Sci. Eng. Appl.* **2020**, *12*, 042123. [CrossRef]

3. Ren, Y.J.; Venugopal, V.; Shi, W. Dynamic analysis of a multi-column TLP floating offshore wind turbine with tendon failure scenarios. *Ocean Eng.* **2022**, *245*, 110472. [CrossRef]
4. Ding, H.Y.; Lian, J.J.; Li, A.D.; Zhang, P.Y. One-step-installation of offshore wind turbine on large-scale bucket-top-bearing bucket foundation. *Trans. Tianjin Univ.* **2013**, *19*, 188–194. [CrossRef]
5. Zhang, P.Y.; He, S.H.; Liu, Y.G. Force transfer characteristics of composite bucket foundation for offshore wind turbines. *J. Renew. Sustain. Energy* **2016**, *8*, 013307. [CrossRef]
6. He, S.; Zhang, P.; Ding, H. Study on the Bearing Mode and Force Transfer Path of composite bucket foundations. *Energies* **2017**, *10*, 1041. [CrossRef]
7. Jia, N.; Zhang, P.; Liu, Y.; Ding, H. Bearing capacity of composite bucket foundations for offshore wind turbines in silty sand. *Ocean Eng.* **2018**, *151*, 1–11. [CrossRef]
8. Zhao, X.; Zhang, P.; Lv, Y.; Ding, H. Scour effects on bearing capacity of composite bucket foundation for offshore wind turbines. *Mar. Georesour. Geotechnol.* **2020**, *38*, 223–237. [CrossRef]
9. Seidl, L.H. Development of an ASP (Air Stabilized Platform). *NASA STI/Recon Technical Rep. N* **1980**, *81*, 14183.
10. Pinkster, J.; Scholte, E.M. The behaviour of a large air-supported MOB at sea. *Mar. Struct.* **2001**, *14*, 163–179. [CrossRef]
11. Lee, C.H.; Newman, J.N. Wave effects on large floating structures with air cushions. *J. Mar. Struct.* **2000**, *13*, 315–330. [CrossRef]
12. Bie, S.; Xu, Y.; Wang, G. Study on floating state and kinetic properties of the air floated structures. *J. Tsinghua Univ.* **2001**, *41*, 123–126.
13. Bie, S.; Shi, Z.; Wang, L. Stability analysis of air float structuers with small roll angle. *China Harb. Eng.* **2001**, *2*, 31–36.
14. Lian, J.J.; Chen, F.; Wang, H.J. Laboratory tests on soil–skirt interaction and penetration resistance of suction caissons during installation in sand. *Ocean Eng.* **2014**, *84*, 1–13. [CrossRef]
15. Zhang, P.; Hu, R.; Ding, H.; Guo, Y.; Xiong, K. Comparative analysis of seepage field characteristics in bucket foundation with and without compartments. *Ocean Eng.* **2017**, *143*, 34–49. [CrossRef]
16. Hu, R.; Zhang, P.; Ding, H.; Le, C. Numerical analysis of seepage field of bucket foundations for offshore wind turbines. *Ships Offshore Struct.* **2018**, *13*, 822–834. [CrossRef]
17. Zhang, P.; Wei, W.; Jia, N.; Ding, H.; Liu, R. Effect of seepage on the penetration resistance of bucket foundations with bulkheads for offshore wind turbines in sand. *Ocean Eng.* **2018**, *156*, 82–92. [CrossRef]
18. Ding, H.Y.; Huang, X.; Zhang, P.Y.; Liu, X.Q. Analysis on influence factors of towing of air float bucket foundation platform. *Eng. Mech.* **2012**, *29*, 193–198.
19. Zhang, P.Y.; Ding, H.Y.; Le, C.H.; Huang, X. Towing characteristics of large-scale composite bucket foundation for offshore wind turbines. *J. Southeast Univ.* **2013**, *3*, 300–304.
20. Zhang, P.Y.; Han, Y.Q.; Ding, H.Y.; Zhang, S.Y. Field experiments on wet tows of an integrated transportation and installation vessel with two bucket foundations for offshore wind turbines. *Ocean Eng.* **2015**, *108*, 769–777. [CrossRef]
21. He, F.; Huang, Z.; Law, A.W.-K. An experimental study of a floating breakwater with asymmetric pneumatic chambers for wave energy extraction. *Appl. Energy* **2013**, *106*, 222–231. [CrossRef]
22. Bie, S.A.; Ren, Z.J.; Li, Z.Z. Mechanical Properties of Air Floating Structures. *Chin. J. Appl. Mech.* **2004**, *1*, 68–71.
23. Ding, H.; Zhao, X.; Le, C.; Zhang, P.; Min, Q. Towing Motion Characteristics of Composite Bucket Foundation for Offshore Wind Turbines. *Energies* **2019**, *12*, 3767. [CrossRef]
24. Zhang, P.Y.; Shi, J.C.; Ding, H.Y.; Huang, X.X. Floating analysis of composite bucket foundation of offshore wind turbine. *Acta Energ. Sol. Sin.* **2014**, *35*, 2313–2319.
25. Zhang, P.Y.; Zhao, X.; Ding, H.Y.; Le, C.H. The wet-towing resistance of the composite bucket foundation for offshore wind turbines. *Marine Struct.* **2021**, *80*, 103089. [CrossRef]
26. Ding, H.Y.; Feng, Z.T.; Zhang, P.Y.; Le, C.; Guo, Y. Floating performance of a composite bucket foundation with an offshore wind tower during transportation. *Energies* **2020**, *13*, 882. [CrossRef]